

## ASSESSMENT OF FUEL CLADDING INTEGRITY BY THE SEGMENTED EXPANDING MANDREL (SEM) TEST

K-F.Nilsson<sup>1</sup>, M. Negyesi<sup>2</sup>

<sup>1</sup>European Commission, DG-JRC, Institute for Energy, PO Box 2, 1755 ZG, Petten, The Netherlands

<sup>2</sup>Dep. of Materials, Faculty of Nucl. Sci. and Physical Engineering, Czech Tech. Univ. in Prague, Czech Rep.

E-mail of corresponding author: karl-fredrik.nilsson@jrc.nl

### ABSTRACT

This paper presents the segmented expanding mandrel test as a materials characterization test as well as a test to simulate pellet cladding interaction. It is shown that the test can be used to derive stress-strain curves at moderate plastic deformation provided the friction coefficients are low and known. The pellet-cladding can be simulated by selecting representative friction coefficients and segments to represent cracked fuel. The test used limited amount of material and it is simple to perform. In particular the test can be used quantify how defects assess the ductility of thin-walled cladding tubes.

### INTRODUCTION

Fuel claddings provide a primary safety function as they constitute the first barrier against release of radionuclides. There exist no standard methods for determining basic material properties for thin-walled cladding tubes or for tests that can simulate the key features of fuel pellet cladding interaction. A material characterization test should be as simple as possible to analyse, and preferably deform in a stable manner under softening or defect growth. A test with axisymmetric displacement controlled loading would be ideal. A test to simulate pellet-cladding interaction should include the key interaction features. When the fuel is put into the reactor there is a small gap between the fuel pellets and the inner surface of the cladding tube. The cladding diameter shrinks from the external pressure by creep and at the same time the fuel expands thermally and by swelling whereby fuel and cladding tube come in contact. The fuel pellets have very strong radial temperature gradients (100° C/mm) which leads to differential thermal expansion, which causes hourglassing and fragmentation of the fuel pellets with primarily radial cracks after a few cycles. The number of cracked fuel segments around the circumference is typically 4 – 10. The fuel cracking and hourglassing lead to stress and strain concentrations which may promote initiation of cracks and clad failure at the location of the fuel crack. In this paper we will explore the segmented expanding cone-mandrel (SEM) test both as a material characterization test and as a test to simulate the mechanical pellet-clad interaction. We will illustrate the application by investigating the ductility of zirconium alloys with re-oriented hydrides.

### DESCRIPTION OF THE SEGMENTED EXPANDING MANDREL (SEM) TEST

The segmented expanded cone-mandrel (SEM) test was proposed in the eighties [1]. Figure 1a shows the principles of our test set-up [2]. A set of segments are manufactured from a cylindrical specimen. The outer radius should be equal to the inner radius of the tube to be tested. A conical volume with the same angle as the cone is removed from the central part of the cylinder. The cylinder is then cut into equal sized segments. When the cone is displaced vertically by a specific value,  $u_z$ , a corresponding radial displacement,  $u_r = \tan(\theta/2) \cdot u_z$ , is imposed on the segments and the inner surface of the tube. The segments do not carry any hoop stress and have a very small deformation. The tube will be subjected to a periodic but controlled radial displacement from the segments. At the segment edges more complex stress and strain concentration occur that depend strongly on the friction between the segments and the cladding tube. As a component test it is desirable that the stress variations induced by the segments are representative whereas for a material characterization test one would like to minimize them. Different loadings can be obtained by controlling the number of segments and the friction coefficient. The deformation becomes more axi-symmetric by increasing the number of segments and by reduced friction between the tube and the segments.

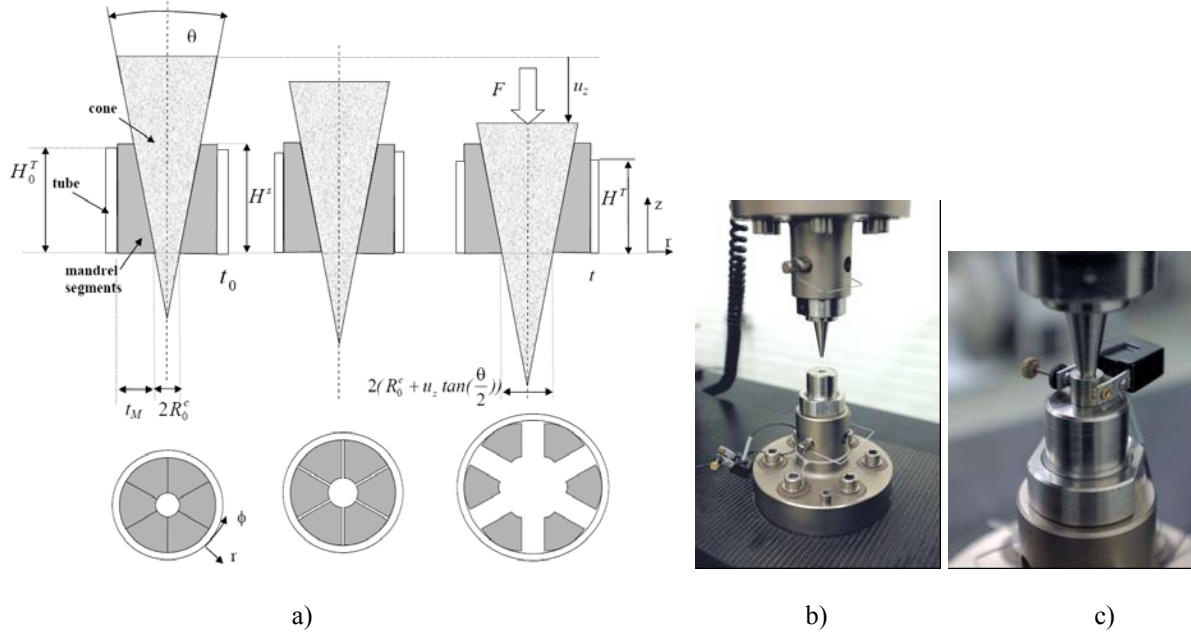


Figure 1 a) Schematic illustration of the principles for the cone mandrel test before loading and with 5% and 50% applied strain b) loading device with cylindrical block, cone, segments and cladding tube c) loaded specimen with extensometer for strain measurement

Figure 1b and 1c show the set-up and a tube with segments and cone ready for testing. The designed prototype for the experiment consists of a lower cylindrical block, a cone with angle  $20^\circ$  and sets of segments. The segments and cone were made from STAVAX, which is a very hard and wear resistant material. The height and outer diameter of the cylinder from which the segments are made are 9.7 mm and 9.2 mm respectively. The diameter of the cylindrical hole at the bottom is 2.8 mm and at the upper end it is 6.2 mm to fit the cone. The lower block has a hole with a diameter suitable to allow enough travel for the cone to move down into it, whilst still providing a sufficient support for the assembly of segments and tube with pure sliding. The vertical displacement and the reaction force are recorded during loading and the change in diameter is measured by a transverse extensometer. The contact surfaces were sprayed with teflon to minimize friction.

#### MODELS: AXISYMMETRIC SEMI-ANALYTICAL MODEL AND 2D FINITE ELEMENT MODEL

The deformation and associated stress distribution is clearly three-dimensional. In order to highlight some salient features we will apply a simplified axi-symmetric analytical model to assess how the friction between cone/segment, segment/block and segment/tube influence the reaction force and a two-dimensional finite element model for assessment of the segment tube interaction. For more detailed descriptions see [2].

##### Axi-symmetric semi-analytical model

The analysis is based on the following assumptions: i) the deformation and loading are axi-symmetric; ii) the cone and the segments are rigid but the segments do not carry any hoop stresses; iii) the contact model is a simple Coulumb friction where the ratio between the tangential and normal component is equal to the friction coefficient ( $p_t / p_N = \mu$ ); iv) the tube has constant hoop stress and is stress free in the axial direction ( $\sigma_z = 0$ ) and the radial stress is much smaller than the hoop stress and set to zero ( $\sigma_r = 0$ ) and there are no shear stresses; v) the material possesses orthotropic symmetry and plastic deformation is assumed to follow the Hill classic quadratic yield criterion, which we express in the form:

$$f(\sigma_{ij}) = \sqrt{\frac{3}{2}} \sqrt{\frac{F(\sigma_{11} - \sigma_{22})^2 + G(\sigma_{22} - \sigma_{33})^2 + H(\sigma_{11} - \sigma_{33})^2 + 2L\tau_{12}^2 + 2M\tau_{23}^2 + 2N\tau_{13}^2}{F + G + H}} - \sqrt{\frac{3(G + H)}{2(F + G + H)}} h(\epsilon_{ij}^p) = 0, \quad (1)$$

and the plastic strain increments are given by,

$$d\epsilon_{ij}^p = d\lambda \frac{\partial f(\sigma_{ij})}{\partial \sigma_{ij}} = \begin{cases} d\epsilon_{11}^p = d\lambda [F(\sigma_{11} - \sigma_{22}) + H(\sigma_{11} - \sigma_{33})], & d\epsilon_{12} = d\lambda 2L\tau_{12} \\ d\epsilon_{22}^p = d\lambda [G(\sigma_{22} - \sigma_{33}) + F(\sigma_{22} - \sigma_{11})], & d\epsilon_{23} = d\lambda 2M\tau_{23} \\ d\epsilon_{33}^p = d\lambda [H(\sigma_{33} - \sigma_{11}) + G(\sigma_{33} - \sigma_{22})], & d\epsilon_{13} = d\lambda 2N\tau_{13} \end{cases} \quad (2)$$

$F, G, H, L, M$  and  $N$  are anisotropy parameters,  $h(\epsilon_{ij}^p)$  is a function describing the isotropic hardening and  $d\lambda$  is a scalar factor for proportional loading. For  $F = G = H = 1$  and  $L = M = N = 3$ , this yield function is simplified to the isotropic von Mises yield function. The basic assumptions and equilibrium leads to a set of linear equations. The known variables (see Figure 1) are: the initial height ( $H_0^T$ ) and thickness ( $t_0$ ) of the cladding tube, the diameter ( $2R_0^c$ ) and thickness ( $t_M$ ) of the segments' lower part and the height of the segment ( $H^s$ ), the angle of the cone ( $\theta$ ), the vertical displacement ( $u_z$ ) and associated force ( $F_z$ ) and the friction coefficient between the different friction surfaces ( $\mu_1, \mu_2, \mu_3$ ). The unknowns are: the contact pressures ( $p_1, p_2, p_3$ ), the hoop stress,  $\sigma_\theta$ , the height ( $H^T$ ) and wall thickness ( $t$ ) of the tube. The subscript 1, 2 and 3 for pressure and friction refer to cone/segment, segment/tube and segment/block contact surfaces respectively. The resulting equations are:

$$\left. \begin{aligned} \epsilon_{\phi\phi} = \ln\left(1 + \frac{u_z \tan(\theta/2)}{R_0^c + t_M}\right), \quad H^T = H_0^T \left(1 + \frac{u_z \tan(\theta/2)}{R_0^c + t_M}\right)^{\frac{-F}{F+G}}, \quad t = t_0 \left(1 + \frac{u_z \tan(\theta/2)}{R_0^c + t_M}\right)^{\frac{-G}{F+G}} \\ p_1 = \frac{F_z}{A_c^{\text{Pr}}(1 + \mu_1/\tan(\theta/2))}, \quad p_3 = \frac{F_z [1 + \mu_2 \left(\frac{1 - \mu_1 \tan(\theta/2)}{\tan(\theta/2) + 1}\right)]}{A_M^{\text{Pr}}(1 + \mu_3 \mu_2)}, \quad p_2 = \frac{F_z}{A_L^T} \left[ \frac{1 - \mu_1 \tan(\theta/2)}{\tan(\theta/2) + 1} - \mu_3 \frac{1 + \mu_2 \frac{1 - \mu_1 \tan(\theta/2)}{\tan(\theta/2) + 1}}{1 + \mu_1 \mu_2} \right] \\ A_c^{\text{Pr}} = \pi[(H_0^s \tan(\theta/2) + R_0^c) - R_0^c]^2, \quad A_M^{\text{Pr}} = \pi[(H_0^s + R_0^c) - R_0^c]^2, \quad A_L^T = 2\pi H_0^T (R_0^c + t_M) \left(1 + \frac{u_z \tan(\theta/2)}{R_0^c + t_M}\right)^{\frac{-F}{F+G}}, \\ \sigma_\theta = \frac{p_2(t_M + R_0^c)}{t} \end{aligned} \right\} \quad (3)$$

**2D FE-Model**

A 2D ABAQUS finite element model was adopted to assess the periodic variation induced by the segments. To this end half a segment is meshed with appropriate boundary and symmetry conditions as shown in Figure 2a. Figure 2b shows the stress-strain curve used in the analysis. This is a typical stress-strain curve for re-crystallized zircaloy-2 at room temperature. Coulumb friction is assumed in the contact zone between tube and cone.

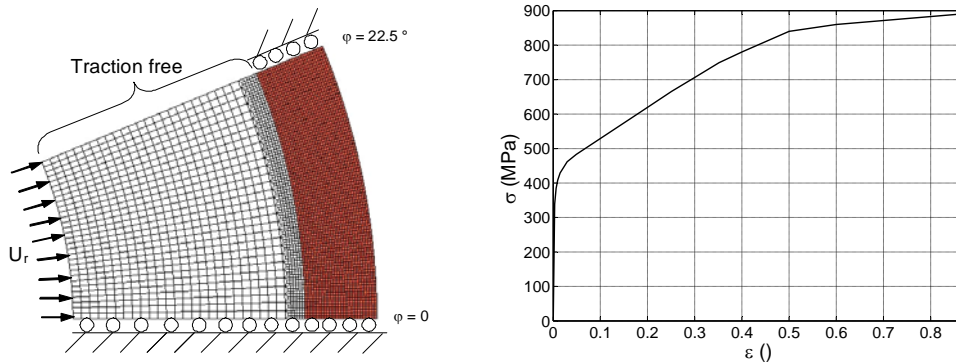


Figure 2: The finite element and associated boundary conditions model for the 8-segment mandrel and tube b) Typical true stress-strain curves for recrystallized Zircaloy-2 used in the FE-analysis

**ASSESSMENT OF KEY PARAMETERS (# OF SEGMENTS, FRICTION)**

Figure 3a shows the measured reaction forces versus the normalized radial displacement for six different tests. The first number in the legend (6, 8, 10 or 12) indicates the number of segments. The difference between the curves could stem from variation in the tensile properties between the tested tubes or from variability of the test method itself. For instance it is obvious that the alignment of the segments between the tests may vary a bit and the friction between the different surfaces may also vary between tests. Nevertheless the variation is not very large. Figure 3b shows the computed stress-strain curves from the measured displacement and forces of test 8-4 using equation (1) – (3) for seven different values of the friction coefficient (0 to 0.3). The same friction coefficient is assumed between all contact surfaces and the material is assumed to be isotropic. The symbols represent the ‘typical data’ also shown in Figure 2b. A typical friction coefficient for teflon is 0.04 and we note that the computed curve with this value agrees quite well with the typical curve for this friction coefficient. In Figure 2c the stress strain curves computed with a friction value of 0.4 are plotted for all six specimens. The curves diverge more at higher loads when localized plastic deformation develops. Figure 3c shows the computed stress-strain curves from the data from test 8-4 for four different friction cases; one when the friction coefficient is 0.2 for each of the three contact surfaces and in the other cases it is 0.2 for two surfaces and 0 for one. The most important observation is that the friction has by far the largest effect for the cone/segment surface.

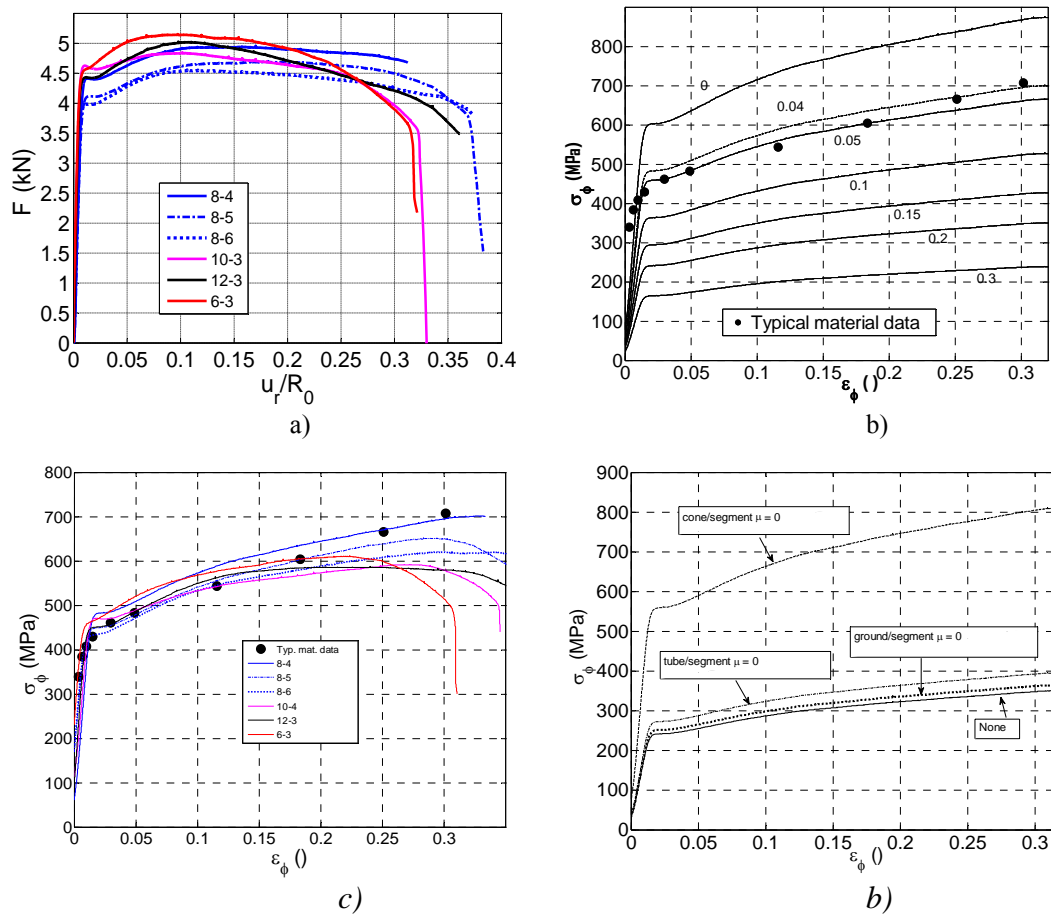


Figure 3 a) Measured reaction force vs. applied radial displacement; computed hoop stress-strain curve using the axi-symmetric analytical model and measured forces and displacement b) Test 8-4 with different values of the friction coefficient but equal for all contact c) all test tests with hard cone and friction coefficient = 0.04 d) friction coefficient 0.2 for all surfaces (None) and 0.2 for all but the surface indicated in the Figure

The effect of stress concentration induced at the edge of the segments and friction using the 2D plain strain model are illustrated in Figure 4 where the hoop strain distributions along the interface with segment/tube friction coefficient between 0 and 0.5 are plotted along the inner and outer surfaces of the tube. It is clear that the friction coefficient has a very large effect on the strain distribution and the peak value, and that this variation is larger along the inside. The value 0.5 is a typical value for pellet-cladding prior to any irradiation and gives a local stress

concentration factor of 2.5. As the fuel becomes irradiated the friction coefficient increases and the stress concentration effect becomes stronger. Such stress concentrations must be accounted for in a safety analysis.

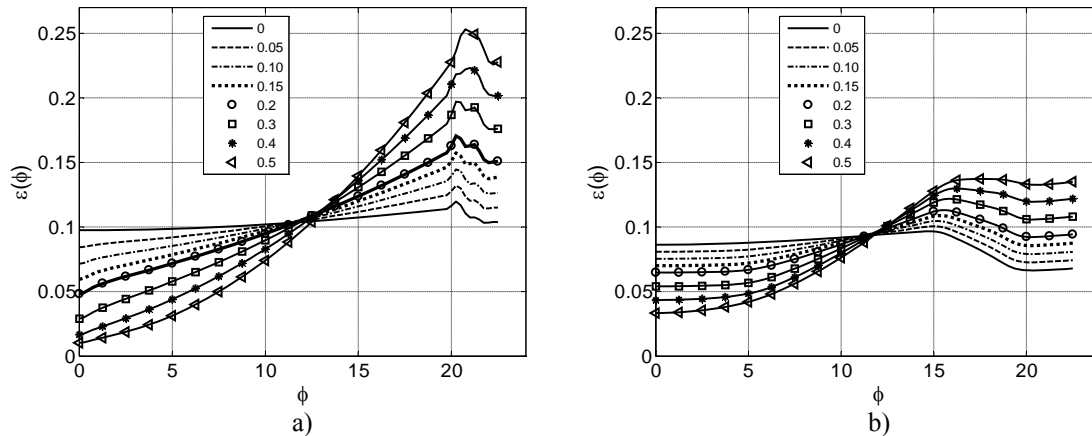


Figure 4 Hoop strain distributions at 10% applied strain for different values of the friction coefficient with 8 segments a) inner surface b) outer surface

The number of segments as well as the friction coefficient has a large impact on the variation in the tube’s stress and strain distributions. The computed plastic effective strain distribution in the tube and cone at an applied engineering strain of 26% is plotted in Figure 5a and 5b for the case with 12 segments and zero friction coefficient and 8 segments and friction coefficient 0.5 respectively. With friction the highest strain in the tube develops in the gap between the segments as clearly seen in Figure 5b. Most of the overall plastic strain takes place in these regions with large deformation and low hardening. This plastic strain localization is the reason why the computed stress strain curves from the mandrel test as outlined above and illustrated in Figure 3 underestimates the plastic hardening at large strains. This effect increases with higher friction and fewer segments. It can also be noted that there is some plastic deformation at the inner segment corner. This may influence the load distribution since the curvature does not match the cone. It could also lead to fatigue damage segment after many test cycles. More details can be found in [2].

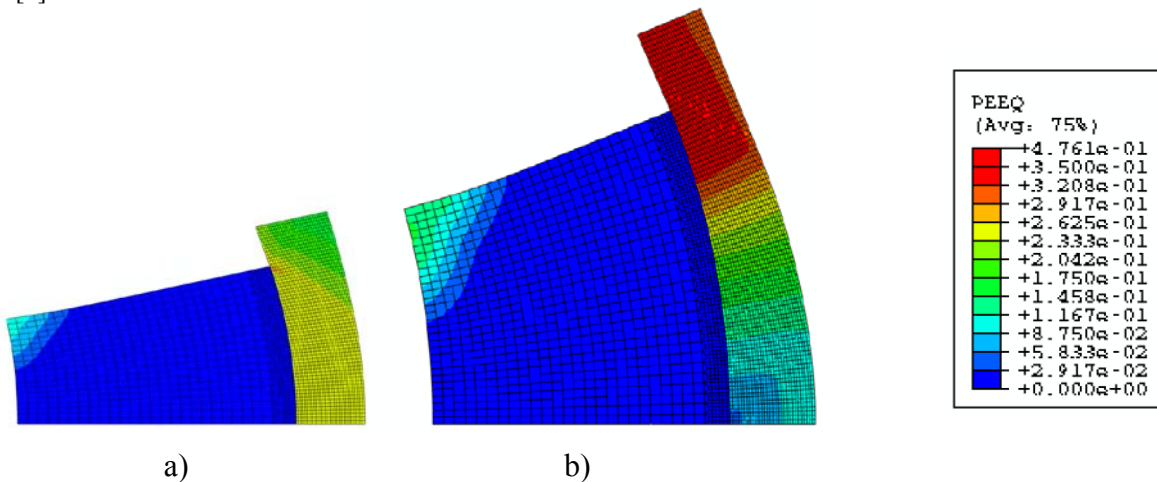


Figure 5 Computed plastic effective strain in segment and tube at applied radial displacement  $u_r/R_0 = 0.26$  a) 12 segments,  $\mu = 0$  b) 8 segments,  $\mu = 0.5$

### APPLICATION: HYDRIDE REORIENTATION AND EMBRITTEMENT IN ZIRCALOY

Zirconium alloy fuel cladding pick up hydrogen from corrosion during reactor operation. When the spent fuel is cooled in water pools the hydrogen precipitates as hydrides with primarily circumferential orientation due to the texture of the cladding tube. When the spent fuel is transferred from wet to dry storage the temperature increases to

typically 400°C whereby the hydrides dissolve and the internal pressure in the cladding tubes increases to 6-16 MPa. When the cladding tubes are slowly cooled the hydrogen reprecipitates as radial hydrides due to the hoop stress [3][4]. At 400°C, the typical threshold value for hydride re-orientation is 60-100 MPa [4], which is achieved from the internal pressure in the fuel claddings. The hydrides are much more brittle than the matrix material when the temperature is below 300°C. It has been observed that radial hydrides may drastically reduce the ductility of fuel claddings at low temperatures [3][4]. The ductility reduction is believed to be caused by a process where first hydrides fracture (typically at 1% strain) whereby the cladding tubes becomes a multi-cracked material. Elastoplastic fracture mechanics can then be applied to assess the ductility [5].

We used the mandrel test for hydride re-orientation as well as the ductility test. To this end zircaloy-2 tubes that had been charged with nominal hydrogen content 100, 200 and 300 ppm were used.

### Hydride Re-Orientation Test

The re-orientation was done as follows: The tube was loaded in load control using the SEM-test to an estimated hoop stress of 150 MPa using the applied force and the axi-symmetric model and an assumed friction coefficient of 0.05. The temperature was increased linearly for 35 minutes to a maximum temperature of 400 °C or 450 °C. This temperature was then kept constant for 60, 120 or 240 minutes. The temperature was subsequently reduced linearly with a rate ranging between 0.5 and 1.5 °C/minute to an end temperature between 30 °C to 175 °C. All in all 30 re-orientation tests were performed. The temperature cycle was performed once or twice and in one case four times. The details of these tests are reported in [6].

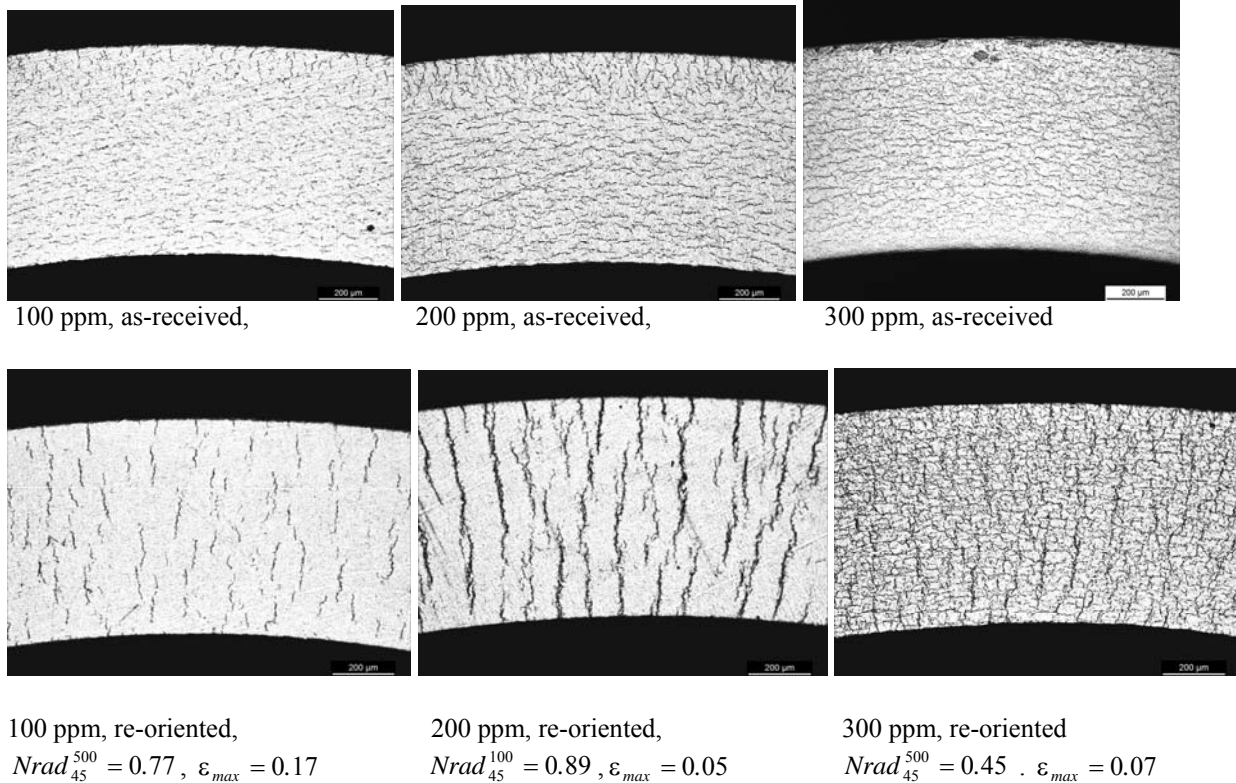


Figure 6 Examples of micrographs of tubes with nominally 100, 200 and 300 ppm hydrogen before and after re-orientation test. The re-orientation and hoop strain at failure are given for the re-oriented specimens.

Examples of micrographs with 100, 200 and 300 ppm hydrogen content before and after re-orientation are shown in Figure 6. The re-orientation is obvious from the naked eye observation of the micrographs. The hydrides were mapped from micrographs with matlab based in-house image processing routines. Each individual hydride exceeding a threshold length was identified with respect to orientation, length and position. There is no agreed definition on hydride re-orientation. We consider hydrides that have an orientation larger than 45° from the circumferential direction as re-oriented. The re-orientation and other hydride parameters are derived from the image processing. The values depend on some internal settings and the magnification of the micrographs. The resulting re-

orientation level decreases generally with lower magnification. We used magnification factors of 500, 200 or 100. The re-orientation for the 200 ppm specimen in Figure 6 was 0.89 with magnification 100 and 0.73 with magnification 500. The length of hydrides also increases after re-orientation.

**Ductility test**

Thirty four tubes were tested at room temperature using the mandrel test under displacement control to determine the failure load. There were two specimens with no hydrogen, 9 with 100 ppm, 7 with 200 ppm and 16 with 300 ppm. One of the 200 ppm and two of the 300 ppm specimens had not undergone re-orientation. The failure hoop strain was about 30% for the specimens with no hydrogen and for the non-reoriented specimens. As expected, the ductility was reduced for the specimens with re-oriented hydrides. The assumed mechanism for the ductility reduction is as follows [5]: i) the hydrides are brittle at room temperature and fracture at a relatively low load (typically 1% strain); ii) fractured hydrides become cracks; iii) the large number of cracks interact and failure occurs when the ligaments between a number of cracked hydrides yield across the wall thickness and the tubes loses its residual strength. The reduction in ductility depends on the hydride configuration in a complex manner. Important parameters are the of course the number and length of radial hydrides and the radial and circumferential distance between neighbouring cracked hydrides. Figure 7a and 7b show the ductility versus the fraction of radial hydrides (measured as those more than 45° from the circumferential direction) and the average length of radial hydrides. Figure 7c plots the radial hydride fractions multiplied with the hydride content; hence this is a measure of the amount of radial hydrides and gives as expected a better trend.

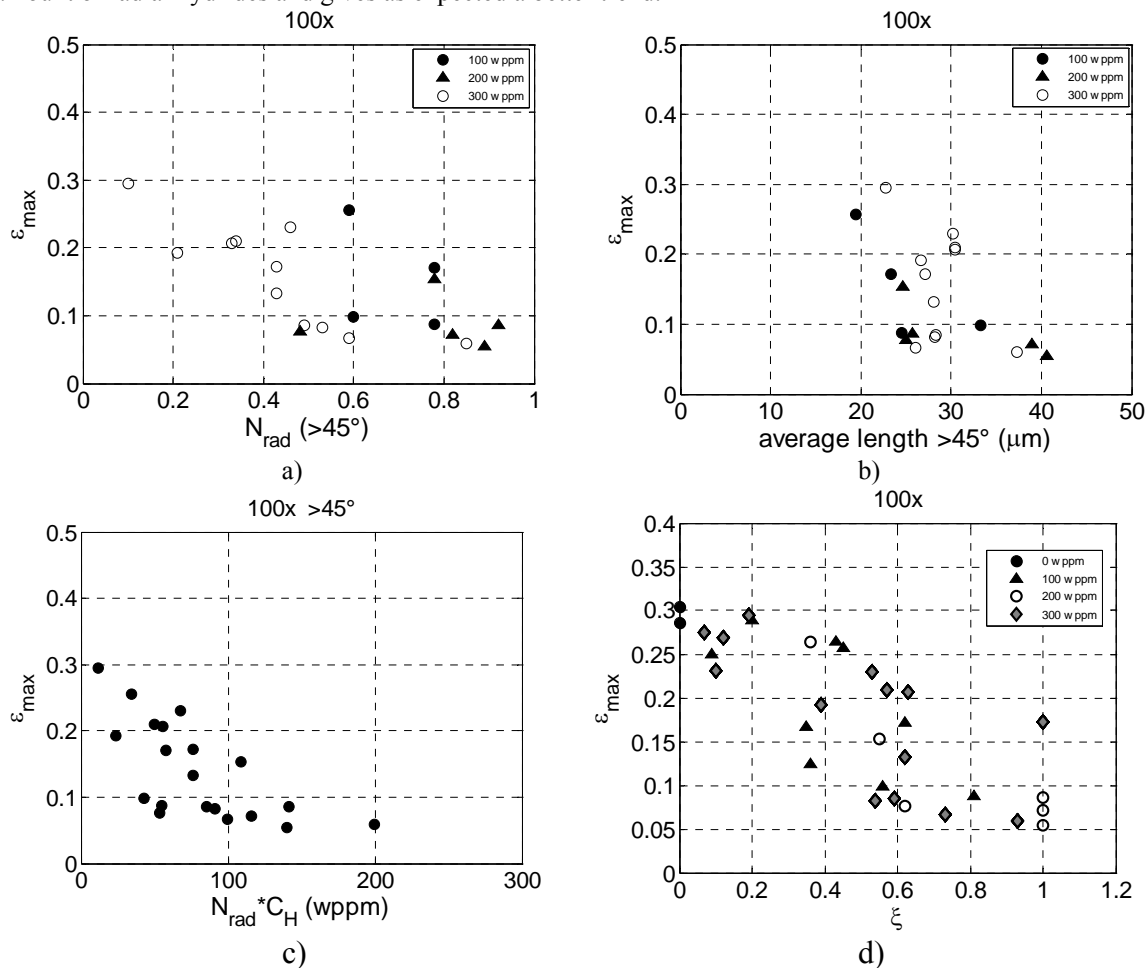


Figure 7 Measured hoop strain at failure versus different parameters a) fraction of radial hydrides (> 45°) b) mean length of radial hydrides c) radial hydride fraction times hydride content d) length fraction of hydrides (> 70°) across thickness.

The fracture mechanics based model [5] suggests that the most deleterious hydride configuration is when a set of aligned radial hydrides within a narrow circumferential band cover a large fraction of the wall thickness. This can be expressed by  $\xi = \sum_1^N a_i/t$ , where  $a_i$  is the length of individual radial hydrides and  $t$  the wall thickness. Figure 7c shows the ductility versus  $\xi$ , where  $\xi$  has been determined from the hydrides with an angle larger than 70° within circumferential bands of width 20 mm around the tube's circumference. The trend is similar to Figure 7b. It should also be noted based on fracture mechanics analysis neighbouring hydrides may also interact so the failure load increases if the tips hydrides overlap in the radial direction [5]. It is our intention to perform more detailed fracture analysis using the specific crack configurations as input. Fracture surfaces from fractographic analysis displayed fractured hydrides joined by zones of ductile tearing in line with the assumed "ligament yield scenario" between cracked hydrides.

### CONCLUSIONS AND FUTURE DEVELOPMENT

This paper has presented the segmented expanding mandrel (SEM) test that can be used for material characterization as well as to simulate mechanical pellet-cladding interaction. The following preliminary conclusions can be drawn:

- The test results are sensitive to the friction between the different parts. As a material characterization test one would like to minimize friction whereas as a simulation test for pellet-cladding interaction one would like to have representative values.
- The test is very simple to perform and requires limited amount of material (typically 10 mm tubes). This has clear advantages when available material is limited (e.g. irradiated material) or for determining statistical distribution of properties.
- The SEM test can be used to qualitatively assess stress strain curves of cladding tubes provided the friction coefficients are small and known. But the test is better suited to determine critical strains. In combination with image processing tools it is possible to assess the relationship between defects and ductility as demonstrated for hydrides in this paper.

Further applications and developments we have in mind include:

- Installing the bellows based SEM test in corrosion loops to address corrosion induced degradation.
- Designing hourglass shaped segments to represent more realistic pellet-cladding interaction;
- Testing irradiated specimens;
- Introducing bi-axial loadings;
- Dynamic loadings to address strain rate effects.

### REFERENCES

- [1] Nobrega, B.N., King, J.S., Was, G.S., Wisener, S.B., Improvements in the design and analysis of the segmented expanding mandrel test. *J. Nucl. Mater.* 131, (1985), 99-104
- [2] Nilsson, K-F, Martin O., Chenel-Ramos, C., Mendes, J., *Nucl. Engng. Design*, 241, (2011), 445-448
- [3] Marshall, R.P., Louthan Jr., M.R., Tensile properties of zircaloy with oriented hydrides. *ASM Trans. Q.* 56, (1963), 693–702.
- [4] H.C. Chu, S.K. Wu, R.C. Kuo, Hydride re-orientation in Zircaloy-4 cladding, *Journal of Nuclear Materials* 373 (2008) 319-327
- [5] Nilsson, K-F, Jakšić, N and Vokál, V., An elasto-plastic fracture mechanics based model for assessment of hydride embrittlement in zircaloy cladding tubes, *J. Nucl. Materials.*, 396, (2010), 71-85
- [6] Nygesi, M., Characterization of Hydrides Induced Embrittlement of Zr-alloy fuel claddings using Segmented Expanding Mandrel Test, 2011, JRC Scientific Report (under finalization)

### ACKNOWLEDGEMENT

This work has been performed as part of the project MATTINO, which is funded by the European Commission. The image processing routines were developed by Dr. Vratko Vokál and his guidance was very essential.